Zinc isotope fractionation as an indicator of geochemical attenuation processes

Harish Veeramani[1†*], Jane Eagling[1], Julia H. Jamieson-Hanes[1], Lingyi Kong[1], Carol J. Ptacek[1] and David W. Blowes[1]

[1]Department of Earth and Environmental Sciences

University of Waterloo

200 University Avenue West

Waterloo, Ontario

Canada N2L 3G1

*harish.veeramani@uwaterloo.ca

†Present Address:

School of Engineering

University of Glasgow

Glasgow G12 8QQ

United Kingdom

Phone: +44(0)141-330-1839

Email: harish.veeramani@glasgow.ac.uk

Abstract

Isotope ratio measurements have been used to trace environmental processes, especially in subsurface environments. In this study we evaluated the potential to use Zinc (Zn) stable isotope ratios as indicators of attenuation processes including sorption and precipitation. Zn isotope fractionation was observed

during distinctly different precipitation processes. Isotope measurements confirmed an increasing trend in aqueous $\delta^{66}Zn$ in solution during sphalerite (ZnS) formation, but a decreasing trend in $\delta^{66}Zn$ during the precipitation of hydrozincite ($Zn_5(CO_3)_2(OH)_6$) and hopeite ($Zn_3(PO_4)_2{\cdot}4H_2O$). In contrast, time-dependent sorption of Zn onto ferrihydrite at a fixed pH did not cause isotopic fractionation in the solution over the duration of the experiments. These findings suggest potential applications of stable isotope measurements in aqueous environments for determining reaction pathways (*e.g.:* precipitation with common groundwater constituents) leading to Zn attenuation.

1. Introduction

Zinc (Zn) is a first row transition chalcophile metal (d-block) that is ubiquitous in the environment and participates in a diversity of biogeochemical processes in soil, sediments and aquatic settings.[1,2] It is an essential micronutrient at low concentrations[3] and toxic at higher concentrations.[4] Although sorption of Zn is often assumed to be the primary process governing its fate and transport,[5,6] it can precipitate as sphalerite (ZnS), Zn hydroxide ($Zn(OH)_2$), Zn carbonate ($ZnCO_3$), or hydrozincite ($Zn_5(OH)_6(CO_3)_2$) that control its concentrations in the environment.[6,7,8,9,10]

Zinc has a high ionization potential making precise determination of the isotope ratios challenging with conventional thermal ionization mass spectrometry. Advances in high-precision analytical instrumentation such as the multicollector inductively-coupled plasma mass spectrometer[11] (MC-ICP-MS) have enabled the study of non-traditional stable isotope fractionation associated with biogeochemical processes occurring in the environment. Zinc isotopic fractionation has been shown to occur during sorption,[12,13,14] chemical diffusion,[15] and biological incorporation.[16] Isotope fractionation has been reported to range from 0.5 – 1 ‰ in oceanic sediments,[17] and soils and plants.[18] Zinc isotope ratios have been used as indicators of biogeochemical processes, [19, 20] anthropogenic contamination in river water samples,[20] watersheds,[21] wetlands,[22] ore deposits,[23] waste-rock drainage,[24] marine sediments,[17] seawater,[25] and biological materials.[26] Variations in isotopic abundances of transition metals such as Zn in biological and geochemical materials have stirred considerable interest into identifying the underlying mechanisms governing isotope fractionation processes in nature.

The present study reports Zn isotope fractionation associated with attenuation processes that control Zn mobility in the environment. The findings are relevant for interpreting trends in Zn isotopic ratios in aquatic settings and in anticipating changes in water quality.

2. Materials and Methods

The reagents used in the experiments were of ultrapure analytical grade. All labware was acid-washed by soaking in 10% HNO_3 overnight and rinsed five times in high-resistivity (18.2 MΩ·cm) water prior to the experiments.

2.1 Sorption Experiments

2.1.1 Iron Oxide Synthesis

A batch of 2-line ferrihydrite was synthesized according to the method described by Antelo and coworkers.[27] Details of the synthesis are included in the Supporting Information (SI). Samples of ferrihydrite were periodically checked by X-ray diffraction (XRD) to ensure the absence of goethite (Figure S1).

2.1.2 Time-dependent sorption experiment

The sorption experiment was carried out in a 1.9 L batch reactor containing 2 g/L of freshly synthesized ferrihydrite. The mineral was suspended in 1.9 L of 0.1 M KNO_3 that was made using high-resistivity (18.2 MΩ·cm) water. The suspension was equilibrated for 24 hours and stirred continuously while being purged with ultrapure Ar gas to minimize CO_2 intrusion over the course of the experiment. An auto-titrator (Metrohm) was used in the pH stat mode to maintain the pH at 7.2 using 0.05 M NaOH and 0.01 M HCl. Geochemical modeling using the PHREEQC[28] with the WATEQ4 database[29] indicated the solution was undersaturated with respect to $Zn(OH)_2$ at pH values < 7.5 under the experimental conditions. The sorption experiment was initiated by adding an acidic stock solution of $ZnCl_2$ (c.a. 75 μM) to a suspension of ferrihydrite. Samples were withdrawn at specified intervals, centrifuged, filtered using disposable 0.2 μm Polysulfone (PES) filters (VWR 28145-499) and acidified with HNO_3 for cation analysis by inductively-

coupled plasma optical emission spectrometry (ICP-OES; Thermo Scientific iCAP 6500) and Zn isotope ratio determinations.

2.2 Precipitation Experiments and Characterization

The precipitation of selected Zn phases was carried out in a series of batch experiments by adding varying concentrations of counter-anions to acidic and anoxic solutions of $ZnSO_4$ or $ZnCl_2$. The suspensions were allowed to equilibrate for 24 hours inside an anoxic glove box followed by centrifugation and filtration. The filtrate was acidified using ultrapure nitric acid for isotope analysis. Parallel time-dependent precipitation tests were carried out to determine the time to equilibrium. Further details of the precipitation experiments including sample preparation and solid-phase characterization are included in the SI.

2.3 Isotope Analysis

Aqueous samples were prepared for Zn isotopic analysis in a clean laboratory environment and under a HEPA-filtered laminar fume hood following a modified procedure described by Marechal et al.[30] A detailed description of the sample preparation and the MC-ICP-MS parameters are included in the SI. Briefly, all five Zn isotopes (^{64}Zn, ^{66}Zn, ^{68}Zn, ^{67}Zn, ^{70}Zn) were monitored simultaneously, along with ^{62}Ni and ^{72}Ge to correct for isobaric interferences. Instrumental mass bias was corrected using a double-spike technique and the application of a double-nested iterative routine; isotope ratios are reported as $\delta^{66}Zn$ relative to the international Zn isotope standard IRMM 3702, where:

$$\delta^{66}\mathrm{Zn} = \left[\frac{(^{66}\mathrm{Zn}/^{64}\mathrm{Zn})_{sample}}{(^{66}\mathrm{Zn}/^{64}\mathrm{Zn})_{IRMM\ 3702}} - 1\right] \times 1000\,‰ \quad (1)$$

Results were normalized to daily measurements of the IRMM 3702 standard. The uncertainty of the isotope measurements was determined to be ± 0.06 ‰ based on twice root-mean-square difference for

19 pairs of duplicate sample preparations. The $\delta^{66}Zn$ values of the starting solutions of $ZnCl_2$ and $ZnSO_4$ were found to be -0.14 ± 0.03 and -0.21 ± 0.04‰, respectively. The fractionation factors were derived from the experimental results by fitting to Rayleigh distillation models. The magnitude of the isotopic fractionation is measured by the fractionation factor, α:

$$\alpha = R_{product} / R_{reactant} \quad (2)$$

where R is the isotope ratio.

For convenience, the fractionation factors can be expressed in terms of ε, a similar per mil quantity:

$$\varepsilon = (\alpha - 1) \times 1000 \text{ ‰} \quad (3)$$

3. RESULTS AND DISCUSSION

3.1 Zn Sorption and Isotope Fractionation

Aqueous Zn(II) was removed from solution over the course of 24 hours at pH 7.2 (Figure S2). This observation is consistent with previous findings that report Zn removal from solution in this pH range. [13,14] Drifts in pH during the experiment were controlled with an auto-titrator. The sorption of Zn onto ferrihydrite at a pH below the point of zero charge (PZC= 7.96 – 8.0) of ferrihydrite[31,32] is likely due to the formation of inner sphere sorption complexes.[33,34]

The $\delta^{66}Zn$ value of the starting/unreacted solution of $ZnCl_2$ was -0.14 ± 0.03 ‰ relative to the IRMM-3702 standard. The data in Figure 1 has been recalculated relative to the isotopic composition of the starting solution (-0.14 ± 0.03 ‰). The uptake of Zn onto ferrihydrite at a fixed pH did not seem to alter the isotopic ratios as a function of time as indicated by the $\delta^{66}Zn$ values of the residual Zn in solution, which varied between 0.01 and -0.05 ‰ relative to the input solution (Figure 1). This finding differs from an earlier study that reported a depletion of $\delta^{66}Zn$ in solution (-0.02 to -0.59 ‰ relative to the IRMM-3702 standard) during Zn(II) sorption onto ferrihydrite where isotopic equilibrium was reached after 16 h of exposure. [14] In our experiments the aqueous concentration of Zn was observed to decrease continuously over time (Figure S2), suggesting that equilibrium was not attained in this study. This may be due to differences in experimental conditions including a higher solid to liquid ratio (2 g/L vs 1 g/L), lower initial Zn concentration (0.08 mM vs 1 mM) and different Zn salt ($ZnCl_2$ vs $Zn(NO_3)_2$). Consequently the lack of isotopic changes (δ66Zn) observed here could be attributed to kinetic effects. Isotope fractionation associated with sorption has been recognized for several metals, but is highly element specific.[35]

A study investigating pH-dependent sorption of Zn onto pyrolusite, birnessite, and corundum reported decreasing $\delta^{66}Zn$ values for residual Zn in solutions with increasing pH values and increasing $\delta^{66}Zn$ values

during Zn sorption onto goethite.[13] However similar pH-dependent studies have also reported decreasing δ^{66}Zn values in solution during Zn sorption onto ferrihydrite and goethite.[14]

Studies examining sorption of Zn onto amorphous silica present in marine diatoms have reported significantly greater enrichment of lighter Zn isotope (-0.82 ‰ relative to IRMM 3702) in the aqueous phase than that observed in the present study with ferrihydrite.[36] Similarly preferential sorption of the heavy Zn isotope onto manganese oxyhydroxide has also been reported. [37] The isotope fractionation of Zn due to sorption onto mineral surfaces has been shown to depend on various factors, including the ionic strength of the suspension, and aqueous speciation of Zn and the molecular coordination environment.[37,38] Aqueous chloro complexes of zinc preferentially contain light Zn isotopes, and this drives the adsorbed pool to be heavier relative to the bulk solution[37]. Although $ZnCl_2$ was used as the starting solution in the present work, time-dependent changes in the isotopic ratio of Zn during sorption onto ferrihydrite was not observed at pH 7.2. Future work investigating Zn isotope changes due to uptake onto mineral surfaces should examine the effect of ionic strength.

Earlier spectroscopic studies indicated that the Zn ion physically sorbs onto ferrihydrite where it retains its hydration shell resembling the spectrum of aqueous Zn^{2+} irrespective of pH and adsorbate loading.[39] The lack of isotope fractionation observed during the current study could be potentially attributed to the unchanged Zn coordination during its uptake onto ferrihydrite. Alternatively an equilibrium effect favoring heavier isotopes on the mineral surface balanced by a kinetic effect with lighter isotopes moving/reacting faster (or vice versa) could potentially explain the absence of isotope fractionation.

3.2 Zn Precipitate Characterization and Isotope Fractionation

The concentrations of Zn decreased in all the batch precipitation experiments with sulfide, carbonate, and phosphate additions. Increasing concentrations of the counter-anion led to greater removal of Zn

161 from solution (Figure S3). Time-dependent precipitation tests using a fixed counter-anion concentration
162 showed that equilibrium was attained in each experiment within less than 24 hours (Figure S4A). The pH
163 of the Zn carbonate and Zn phosphate suspensions remained circumneutral (Table S1). Geochemical
164 modeling using PHREEQC (WATEQ4 database) indicated that the formation of $Zn(OH)_2$ is not favored at
165 pH values < 7 (Table S1). This condition is particularly important because $Zn(OH)_2$ is known to
166 precipitate more rapidly than $ZnCO_3$.[36] The pH of the sphalerite suspensions increased with increasing
167 sulfide concentration due to the basic nature of Na_2S. Although PHREEQC calculations suggested the
168 formation of Zn sulfide (saturation index 11.93 as a mixture of sphalerite, wurtzite, and amorphous ZnS),
169 it also indicated the formation of $Zn(OH)_2$ (saturation index 0.28) at sulfide concentrations > 7mM (pH >
170 7.15). It is important to note that although the predicted saturation indices indicate the feasibility of a
171 chemical reaction they do not indicate the rate of reaction.[40] SEM examination showed distinct
172 morphology of the ZnS particles (Figure S5) with definite crystal boundaries resembling the bulk
173 structure of sphalerite[41] reported in previous studies. X-ray powder diffraction further indicated the
174 presence of sphalerite (Figure S6) and the absence of $Zn(OH)_2$. These observation suggest that the rate
175 of sphalerite formation was greater than the rate of precipitation of $Zn(OH)_2$ although pH values > 7
176 were recorded in the precipitation tests at higher sulfide concentrations. The observed morphology
177 differs from the framboidal ZnS produced under sulfate reducing conditions in esturine sediments[42] and
178 those found in biofilms.[43]

179 Distinct trends in isotope fractionation were observed during sphalerite precipitation relative to
180 the isotopic composition of the starting $ZnSO_4$ solution ($\delta^{66}Zn$ of -0.21 ± 0.04‰ relative to IRMM 3702).
181 The aqueous $\delta^{66}Zn$ values of the $ZnSO_4$ solution were found to increase systematically with increasing
182 sulfide concentrations during Zn sulfide precipitation (Figure 1) indicating an enrichment of ^{66}Zn with
183 respect to ^{64}Zn. Although these precipitation studies were carried out at room temperature in batch
184 reactors using ultrapure reagents in a simple experimental matrix, the findings are consistent with field-

studies on hydrothermal systems that have also reported enrichment of the heavier isotope in the hydrothermal fluids (-0.54 – 0.36 ‰ relative to IRMM 3702) [44] and consequently inferred the preferential incorporation of lighter Zn isotopes into sphalerite. [23,45] Studying δ^{66}Zn during sphalerite precipitation in the laboratory can thus provide reasonable insights into environmental settings such as hydrothermal vents and ore deposits where factors such as temperature, pressure, composition of the source-rocks and kinetic fractionation have been shown to influence the zinc isotope composition of sphalerite. [43–47]

These findings indicate that aqueous Zn reservoirs may become enriched in heavier isotopes through abiotic precipitation of sphalerite, resulting in mineral phases with relatively light Zn isotope ratios. The stable isotope composition of Zn which occurs naturally in only one redox state may fractionate during precipitation with redox-sensitive species such as sulfur and can also be used as a diagnostic indicator of redox conditions.[47]

The Zn phosphate precipitates appeared as lamella of discrete rosettes composed of square sheets/plates (Figure S5), consistent with earlier studies.[48,49] The powder x-ray diffraction pattern was consistent with hopeite ($Zn_3(PO_4)_2{\cdot}4H_2O$) (Figure S6). The Zn carbonate precipitates were present as irregular aggregates with short, acicular crystals (Figure S5). The x-ray powder diffraction data indicated a structure consistent with hydrozincite ($Zn_5(CO_3)_2(OH)_6$ and $Zn_4CO_3(OH)_6.H_2O$) (Figure S6). The urchin-like morphology has been previously reported for hydrozincite.[50,51] The relatively broad lines on the XRD spectra are indicative of the microcrystalline character of the hydrozincite sample. Hydrozincite and hopeite are environmentally relevant minerals and are known to form during Zn(II) sorption onto hydroxyapatite.[52] Hydrozincite has also been reported to precipitate from mine waters due to the activity of photosynthetic microbes[53] and during the dissolution of ZnO nanoparticles in carbonate-rich water.[54]

Zinc displayed similar isotopic behavior during the precipitation of hydrozincite and hopeite relative to the isotopic composition of the starting solutions (δ^{66}Zn of -0.14 ±0.03 ‰). The aqueous δ^{66}Zn values of the residual $ZnCl_2$ solution were found to decrease during the precipitation of hydrozincite and hopeite with increasing carbonate and phosphate concentrations respectively (Figure 1). The formation of hydrozincite in mine drainage of Rio Naracauli, in Sardinia, Italy has been shown to produce waters with lighter values of δ^{66}Zn consistent with the aqueous ^{66}Zn behavior observed during hydrozincite precipitation in the present study. [55]

The depletion of ^{66}Zn relative to ^{64}Zn in the residual solution during hopeite precipitation is also consistent with studies showing enrichment of ^{66}Zn relative to ^{64}Zn in the root system of plants[26,56] due to the formation of Zn phosphate.[57,58]

Whereas the ^{66}Zn isotope data during Zn precipitation are generally consistent with field observations, future research should focus on the role of other factors on Zn isotope fractionation such as interactions with organic matter, uptake by biota, ionic strength, or sorption onto other mineral surfaces, pH, temperature, redox conditions and solution concentration and speciation. Although kinetic isotope effects can potentially play a role in Zn isotope fractionation under certain conditions, the observed isotopic behavior of Zn in the precipitation tests in this study is primarily attributed to equilibrium effects. The trends in Zn isotope fractionation during time-dependent precipitation tests are similar to the precipitation tests involving varied counter-anion concentrations (Figure S4B).

The isotopic behavior of Zn during the precipitation of the three mineral phases can be described using the Rayleigh fractionation model involving one reservoir and an isolated sink in a closed system. [14,35,59] The isotope fractionation values (ε) for sphalerite, hydrozincite and hopeite were calculated as -0.30‰, +0.18‰, and +0.25‰ respectively. The data tends to deviate slightly from the Rayleigh fractionation model towards smaller F values where a large degree of isotope fraction is

observed (Figure 1). This pattern is commonly observed when there is a finite pool of reactants typical of those in closed systems.

The contrasting Zn isotope behavior observed during sphalerite precipitation vs hydrozincite and hopeite can be used as indicators to deduce information about the composition and provenance of environmental samples.[35] The differences in isotopic behavior can be potentially attributed to differences in the coordination environment of Zn. [60,44] The coordination of Zn(II) in aqueous solution is usually octahedral that is characteristic of first-row transition metals. Zn(II) in sphalerite is tetrahedrally coordinated with sulfur atoms.[61] The tetrahedral coordination with sulfur is different than tetrahedral coordination with oxygen due to the larger atomic radius (0.88 Å) and mass (32.065) of sulfur atoms. In contrast, Zn exhibits a combination of tetrahedral and octahedral coordination during the formation of both hopeite and hydrozincite which can potentially explain the observed differences in Zn isotope behaviour.[61,62,63]

3.4 Environmental Implications

Our study shows that Zn isotope ratios can be used as indicators to study selected precipitation processes that lead to changes in aqueous Zn. The loss of Zn from solution due to sphalerite precipitation can be differentiated from loss due to carbonate/phosphate precipitation and adsorption, because an increase in Zn isotope ratio implies sphalerite precipitation.

Over the past decade passive treatment techniques such as constructed wetlands, *in situ* treatment systems, and permeable reactive barriers (PRBs) have been extensively employed for the remediation of metal-impacted waters.[64] The design of such facilities relies on subsurface flow of water and the maintenance of permeable, anoxic conditions. Organic carbon is utilized in constructed wetland systems and *in situ* treatment systems and PRBs to promote the growth and activity of sulfate reducing organisms, leading to the formation of metal-sulfide minerals including sphalerite. The alkalinity

generated in these biologically mediated systems also promotes the formation of metal carbonate precipitates which could potentially include hydrozincite.[65,66] Zn stable isotope measurements may thus be employed in treatment systems to understand pathways leading to the attenuation of Zn from solution. However a range of other factors such as the presence of organic matter, secondary mineral precipitates, ionic strength and speciation of Zn, could influence the effectiveness of field measurements.[34,37] It is also important to note that although the precipitation results reported here describe equilibrium isotope values, kinetic factors may also play a role in determining Zn isotope fractionation in the environment.

Zn isotope ratios may be affected by processes that occur during weathering and transport. By examining Zn isotope ratios one can potentially differentiate between sources of Zn and processes involving Zn to gain insight into the weathering of mineral deposits and processes leading to Zn immobilization in surrounding areas. The findings presented in this work show the potential to use Zn isotope measurements as a complementary analytical technique to differentiate between dominant processes resulting in Zn attenuation or mobility in the environment.

ACKNOWLEDGEMENTS

We thank Emma Buczolits, Joy Hu, and Heather Shrimpton at the University of Waterloo for their support and assistance. We also thank Lei Zhang and Joseph P. Thomas from the WATLab for assistance with electron microscopy. This project was funded by a Natural Sciences and Engineering Research Council (NSERC) Strategic Project Grant awarded to D. Blowes and C. Ptacek.

ASSOCIATED CONTENT Supporting Information Available: Detailed information on the synthesis and characterization of all the mineral phases is included in the supporting material. This material is available free of charge via the Internet at http://pubs.acs.org.

The authors declare no competing financial interest.

4. References

(1) Cloquet, C.; Carignan, J.; Lehmann, M. F.; Vanhaecke, F. Variation in the isotopic composition of zinc in the natural environment and the use of zinc isotopes in biogeosciences: A review. *Anal. Bioanal. Chem.* **2008**, *390*, 451–463.

(2) Sayen, S.; Guillon, E. Aging effect on Zn retention on a calcareous soil: Column experiments and synchrotron X-ray micro-spectroscopic investigation. *Sci. Total Environ.* **2014**, *487*, 545–556.

(3) Morel, F. M. M.; Reinfelder, J. R.; Roberts, S. B.; Chamberlain, C. P.; Lee, J. G.; Yee, D. Zinc and carbon co-limitation of marine phytoplankton. *Nature* **1994**, *369*, 740–742.

(4) Allen, J. G.; Masters, H. G.; Peet, R. L.; Mullins, K. R.; Lewis, R. D.; Skirrow, S. Z.; Fry, J. Zinc toxicity in ruminants. *J. Comp. Pathol.* **1983**, *93*, 363–377.

(5) Gräfe, M.; Sparks, D. L. Kinetics of zinc and arsenate co-sorption at the goethite-water interface. *Geochim. Cosmochim. Acta* **2005**, *69*, 4573–4595.

(6) Roberts, D. R.; Ford, R. G.; Sparks, D. L. Kinetics and mechanisms of Zn complexation on metal oxides using EXAFS spectroscopy. *J. Colloid Interface Sci.* **2003**, *263*, 364–376.

(7) Nachtegaal, M.; Marcus, M. A.; Sonke, J. E.; Vangronsveld, J.; Livi, K. J. T.; van Der Lelie, D.; Sparks, D. L. Effects of in situ remediation on the speciation and bioavailability of zinc in a smelter contaminated soil. *Geochim. Cosmochim. Acta* **2005**, *69*, 4649–4664.

(8) Saeed, M.; Fox, R. L. Influence of phosphate fertilization on zinc adsorption by tropical soils. *Soil Sci. Soc. Am. J.* **1979**, *43*, 683-686.

(9) Sharpless, R. G.; Wallihan, E. F.; Peterson, F. F. Retention of zinc by some arid zone soil materials treated with zinc sulfate. *Soil Sci. Soc. Am. J.* **1969**, *33*, 901-904.

(10) Schindler, P.; Reinert, M.; Gamsjäger, H. Zur Thermodynamik der metallcarbonate. löslichkeitskonstanten und freie bildungsenthalpien von $ZnCO_3$ und $Zn_5(OH)_6(CO_3)_2$ bei 25°. *Helv. Chim. Acta* **1969**, *52*, 2327–2332.

(11) Wieser, M. E.; Schwieters, J. B. The development of multiple collector mass spectrometry for isotope ratio measurements. *Int. J. Mass Spectrom.* **2005**, *242*, 97–115.

(12) Balistrieri, L. S.; Borrok, D. M.; Wanty, R. B.; Ridley, W. I. Fractionation of Cu and Zn isotopes during adsorption onto amorphous Fe(III) oxyhydroxide: Experimental mixing of acid rock

drainage and ambient river water. *Geochim. Cosmochim. Acta* **2008**, *72*, 311–328.

(13) Pokrovsky, O. S.; Viers, J.; Freydier, R. Zinc stable isotope fractionation during its adsorption on oxides and hydroxides. *J. Colloid Interface Sci.* **2005**, *291*, 192–200.

(14) Juillot, F.; Maréchal, C.; Ponthieu, M.; Cacaly, S.; Morin, G.; Benedetti, M.; Hazemann, J. L.; Proux, O.; Guyot, F. Zn isotopic fractionation caused by sorption on goethite and 2-Lines ferrihydrite. *Geochim. Cosmochim. Acta* **2008**, *72*, 4886–4900.

(15) Rodushkin, I.; Stenberg, A.; Andrén, H.; Malinovsky, D.; Baxter, D. C. Isotopic Fractionation during Diffusion of Transition Metal Ions in Solution. *Anal. Chem.* **2004**, *76*, 2148–2151.

(16) Kafantaris, F. C. A; Borrok, D. M. Zinc isotope fractionation during surface adsorption and intracellular incorporation by bacteria. *Chem. Geol.* **2014**, *366*, 42–51.

(17) Pichat, S.; Douchet, C.; Albarède, F. Zinc isotope variations in deep-sea carbonates from the eastern equatorial Pacific over the last 175 ka. *Earth Planet. Sci. Lett.* **2003**, *210*, 167–178.

(18) Arnold, T.; Schönbächler, M.; Rehkämper, M.; Dong, S.; Zhao, F. J.; Kirk, G. J. D.; Coles, B. J.; Weiss, D. J. Measurement of zinc stable isotope ratios in biogeochemical matrices by double-spike MC-ICPMS and determination of the isotope ratio pool available for plants from soil. *Anal. Bioanal. Chem.* **2010**, *398*, 3115–3125.

(19) Maréchal, C. N.; Nicolas, E.; Douchet, C.; Albarède, F. Abundance of zinc isotopes as a marine biogeochemical tracer. *Geochemistry Geophys. Geosystems* **2000**, *1*, 1-15.

(20) Chen, J.; Gaillardet, J.; Louvat, P. Zinc isotopes in the Seine River waters, France: A probe of anthropogenic contamination. *Environ. Sci. Technol.* **2008**, *42*, 6494–6501.

(21) Borrok, D. M.; Wanty, R. B.; Ian Ridley, W.; Lamothe, P. J.; Kimball, B. a.; Verplanck, P. L.; Runkel, R. L. Application of iron and zinc isotopes to track the sources and mechanisms of metal loading in a mountain watershed. *Appl. Geochemistry* **2009**, *24*, 1270–1277.

(22) Aucour, A.-M.; Bedell, J.-P.; Queyron, M.; Magnin, V.; Testemale, D.; Sarret, G. Dynamics of Zn in an urban wetland soil–plant system: Coupling isotopic and EXAFS approaches. *Geochim. Cosmochim. Acta* **2015**, *160*, 55–69.

(23) Kelley, K. D.; Wilkinson, J. J.; Chapman, J. B.; Crowther, H. L.; Weiss, D. J. Zinc isotopes in sphalerite from base metal deposits in the Red Dog District, Northern Alaska. *Econ. Geol.* **2009**, *104*, 767–773.

(24) Matthies, R.; Blowes, D. The zinc stable isotope signature of waste rock drainage in Arctic Canada. *Appl. Geochemistry* **2014**, *16*, 2014.

(25) Bermin, J.; Vance, D.; Archer, C.; Statham, P. J. The determination of the isotopic composition of Cu and Zn in seawater. *Chem. Geol.* **2006**, *226*, 280–297.

(26) Weiss, D. J.; Mason, T. F. D.; Zhao, F. J.; Kirk, G. J. D.; Coles, B. J.; Horstwood, M. S. a. Isotopic discrimination of zinc in higher plants. *New Phytol.* **2005**, *165*, 703–710.

(27) Antelo, J.; Arce, F.; Fiol, S. Arsenate and phosphate adsorption on ferrihydrite nanoparticles. Synergetic interaction with calcium ions. *Chem. Geol.* **2015**, *410*, 53–62.

(28) Parkhurst, D. L.; Appelo, C. A. J. *User's guide to PHREEQC (Version 2) : A computer program for speciation, batch-reaction, one-dimensional transport, and inverse geochemical calculations*, - ed.; 1999.

(29) Ball, J. W.; Nordstrom, D. K. *WATEQ4F -- User's manual with revised thermodynamic data base and test cases for calculating speciation of major, trace and redox elements in natural waters*, - ed.; 1991.

(30) Maréchal, C. N.; Télouk, P.; Albarède, F. Precise analysis of copper and zinc isotopic compositions by plasma-source mass spectrometry. *Chem. Geol.* **1999**, *156*, 251–273.

(31) Brinza, L.; Benning, L. G.; Statham, P. J. Adsorption studies of Mo and V onto ferrihydrite. *Mineral. Mag.* **2008**, *72*, 385–388.

(32) Rout, K.; Mohapatra, M.; Anand, S. 2-Line Ferrihydrite: synthesis, characterization and its adsorption behaviour for removal of Pb(II), Cd(II), Cu(II) and Zn(II) from aqueous solutions. *Dalt. Trans.* **2012**, *41*, 3302.

(33) Nachtegaal, M.; Sparks, D. L. Effect of iron oxide coatings on zinc sorption mechanisms at the clay-mineral/water interface. *J. Colloid Interface Sci.* **2004**, *276*, 13–23.

(34) Jouvin, D.; Louvat, P.; Juillot, F.; Maréchal, C. N.; Benedetti, M. F. Zinc isotopic fractionation: Why organic matters. *Environ. Sci. Technol.* **2009**, *43*, 5747–5754.

(35) Wiederhold, J. G. Metal stable isotope signatures as tracers in environmental geochemistry. *Environ. Sci. Technol.* **2015**, *49*, 2606–2624.

(36) Gélabert, A.; Pokrovsky, O. S.; Viers, J.; Schott, J.; Boudou, A.; Feurtet-Mazel, A. Interaction between zinc and freshwater and marine diatom species: Surface complexation and Zn isotope

fractionation. *Geochim. Cosmochim. Acta* **2006**, *70*, 839–857.

(37) Bryan, A. L.; Dong, S.; Wilkes, E. B.; Wasylenki, L. E. Zinc isotope fractionation during adsorption onto Mn oxyhydroxide at low and high ionic strength. *Geochim. Cosmochim. Acta* **2015**, *157*, 182–197.

(38) Little, S. H.; Sherman, D. M.; Vance, D.; Hein, J. R. Molecular controls on Cu and Zn isotopic fractionation in Fe–Mn crusts. *Earth Planet. Sci. Lett.* **2014**, *396*, 213–222.

(39) Trivedi, P.; Axe, L.; Tyson, T. A. An Analysis of Zinc Sorption to Amorphous versus Crystalline Iron Oxides Using XAS. *J. Colloid Interface Sci.* **2001**, *244*, 230–238.

(40) Zhu, C. Geochemical Modeling of Reaction Paths and Geochemical Reaction Networks. *Rev. Mineral. Geochemistry* **2009**, *70*, 533–569.

(41) Jordan, G.; Pokrovsky, O. S.; Bahlo, J.; Guichet, X.; Schlueter, C. Sphalerite dissolution kinetics at low hydrothermal conditions. *Chem. Geol.* **2011**, *286*, 272–279.

(42) Luther, G. W.; Meyerson, a. L.; Krajewski, J. J.; Hires, R. Metal Sulfides in Estuarine Sediments. *J. Sediment. Res.* **1980**, *Vol. 50*, 1117–1120.

(43) Labrenz, M.; Druschel, G. K.; Thomsen-Ebert, T.; Gilbert, B.; Welch, S. a; Kemner, K. M.; Logan, G. a; Summons, R. E.; De Stasio, G.; Bond, P. L.; et al. Formation of sphalerite (ZnS) deposits in natural biofilms of sulfate-reducing bacteria. *Science* **2000**, *290*, 1744–1747.

(44) John, S. G.; Rouxel, O. J.; Craddock, P. R.; Engwall, A. M.; Boyle, E. A. Zinc stable isotopes in seafloor hydrothermal vent fluids and chimneys. *Earth Planet. Sci. Lett.* **2008**, *269*, 17–28.

(45) Wilkinson, J. J.; Weiss, D. J.; Mason, T. F. D.; Coles, B. J. Zinc isotope variation in hydrothermal systems: Preliminary evidence from the Irish midlands ore field. *Econ. Geol.* **2005**, *100*, 583–590.

(46) Pašava, J.; Tornos, F.; Chrastný, V. Zinc and sulfur isotope variation in sphalerite from carbonate-hosted zinc deposits, Cantabria, Spain. *Miner. Depos.* **2014**, *49*, 797–807.

(47) Schauble, E. Applying stable isotope fractionation theory to new systems. *Rev. Mineral. Geochemistry* **2004**, *55*, 65.

(48) Giuseppina, A.; Emma, A.; Paolo, B.; Gianfranca, G. Constitution and corrosion resistance of phosphate protective coatings. *Metall. Sci. Technol.* **1983**, *1*, 58–63.

(49) Bubert, H.; Pulm, H.; Puderbach, H. Investigations on hopeite- and phosphophyllite-containing phosphate coatings on steel. *Microchim. Acta* **1987**, *91*, 355–364.

(50) Chen, M.; Wang, Y.; Song, L.; Gunawan, P.; Zhong, Z.; She, X.; Su, F. Urchin-like ZnO microspheres synthesized by thermal decomposition of hydrozincite as a copper catalyst promoter for the Rochow reaction. *RSC Adv.* **2012**, *2*, 4164.

(51) De Giudici, G.; Podda, F.; Sanna, R.; Musu, E.; Tombolini, R.; Cannas, C.; Musinu, A.; Casu, M. Structural properties of biologically controlled hydrozincite: An HRTEM and NMR spectroscopic study. *Am. Mineral.* **2009**, *94*, 1698–1706.

(52) Lee, Y. J.; Elzinga, E. J.; Reeder, R. J. Sorption mechanisms of zinc on hydroxyapatite: Systematic uptake studies and EXAFS spectroscopy analysis. *Environ. Sci. Technol.* **2005**, *39*, 4042–4048.

(53) Podda, F.; Zuddas, P.; Minacci, A.; Baldi, F.; Pepi, M. Heavy metal coprecipitation with hydrozincite [$Zn_5(CO_3)_2(OH)_6$] from mine waters caused by photosynthetic microorganisms. *Appl. Environ. Microbiol.* **2000**, *5*, 5092–5098.

(54) Sivry, Y.; Gelabert, a.; Cordier, L.; Ferrari, R.; Lazar, H.; Juillot, F.; Menguy, N.; Benedetti, M. F. Behavior and fate of industrial zinc oxide nanoparticles in a carbonate-rich river water. *Chemosphere* **2014**, *95*, 519–526.

(55) Wanty, R. B.; Podda, F.; De Giudici, G.; Cidu, R.; Lattanzi, P. Zinc isotope and transition-element dynamics accompanying hydrozincite biomineralization in the Rio Naracauli, Sardinia, Italy. *Chem. Geol.* **2013**, *337-338*, 1–10.

(56) Fujii, T.; Albarède, F. Ab initio calculation of the Zn isotope effect in phosphates, citrates, and malates and applications to plants and soil. *PLoS One* **2012**, *7*, e30726.

(57) Sarret, G.; Saumitou-Laprade, P.; Bert, V.; Proux, O.; Hazemann, J.-L.; Traverse, A.; Marcus, M. A.; Manceau, A. Forms of zinc accumulated in the hyperaccumulator *Arabidopsis halleri*. *Plant Physiol.* **2002**, *130*, 1815–1826.

(58) Aucour, A. M.; Pichat, S.; Macnair, M. R.; Oger, P. Fractionation of stable zinc isotopes in the zinc hyperaccumulator *Arabidopsis halleri* and nonaccumulator *Arabidopsis petraea*. *Environ. Sci. Technol.* **2011**, *45*, 9212–9217.

(59) Weiss, D. J.; Harris, C.; Maher, K.; Bullen, T. A teaching exercise to introduce stable isotope fractionation of metals into geochemistry courses. *J. Chem. Educ.* **2013**, *90*, 1014–1017.

(60) Fujii, T.; Moynier, F.; Pons, M. L.; Albarède, F. The origin of Zn isotope fractionation in sulfides. *Geochim. Cosmochim. Acta* **2011**, *75*, 7632–7643.

(61) Vaughan, D.; Tossell, J. Electronic structures of sulfide minerals — Theory and experiment. *Phys. Chem. Miner.* **1983**, *9*, 253–262.

(62) Ghose, S. The crystal structure of hydrozincite, $Zn_5(OH)\cdot 6(CO_3)_2$. *Acta Crystallogr.* **1964**, *17*, 1051–1057.

(63) Liebau, F. Zur Kristallstruktur des Hopeits, $Zn_3(PO_4)_2\cdot 4H_2O$. *Acta Crystallogr.* **1965**, *18*, 352–354.

(64) Obiri-Nyarko, F.; Grajales-Mesa, S. J.; Malina, G. An overview of permeable reactive barriers for in situ sustainable groundwater remediation. *Chemosphere* **2014**, *111*, 243–259.

(65) Remoudaki, E.; Hatzikioseyian, A.; Kousi, P.; Tsezos, M. The mechanism of metals precipitation by biologically generated alkalinity in biofilm reactors. *Water Res.* **2003**, *37*, 3843–3854.

(66) Khoshnoodi, M.; Dipple, G.; Baldwin, S. A. Mineralogical study of a biologically-based treatment system that removes arsenic, zinc and copper from landfill leachate. *Minerals* **2013**, *3*, 427–449.

507 **Figures**

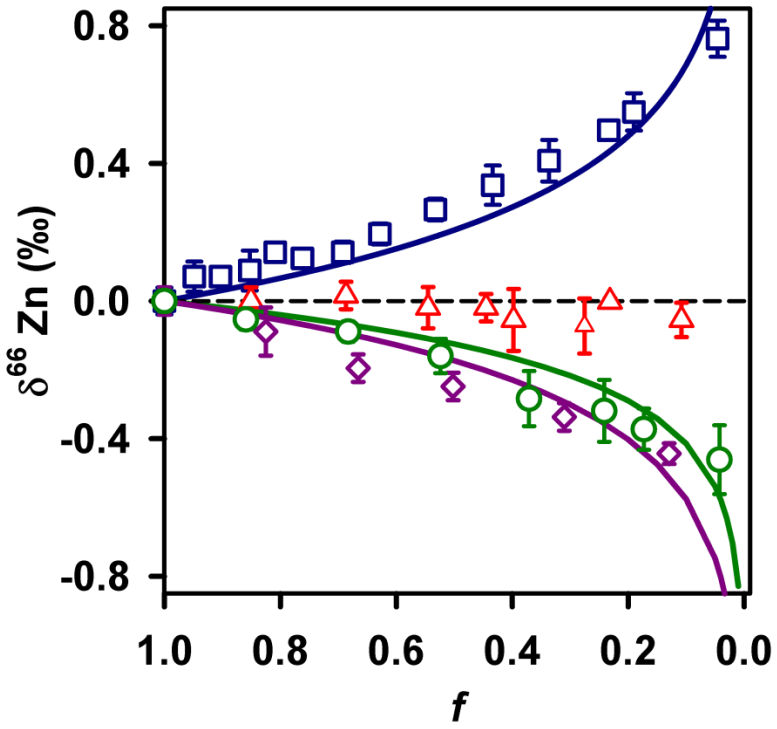

508

509 **Figure 1: Isotope fractionation (δ^{66}) of Zn relative to the input solutions during (△) sorption onto**

510 **ferrihydrite; precipitation of Zn sulfide as sphalerite (□) ε= -0.30 ‰; Zn carbonate as hydrozincite (○)**

511 **ε=0.18‰; and Zn phosphate as hopeite (◇) ε=0.25‰; where f is the fraction of Zn remaining in**

512 **solution. The error bars represent 2σ from three analytical events. The solid blue, green and purple**

513 **lines represent the best-fit Rayleigh models. Symbols where error bars are not seen indicate small**

514 **error bars.**

515

516

517

518 **TOC Graphics**

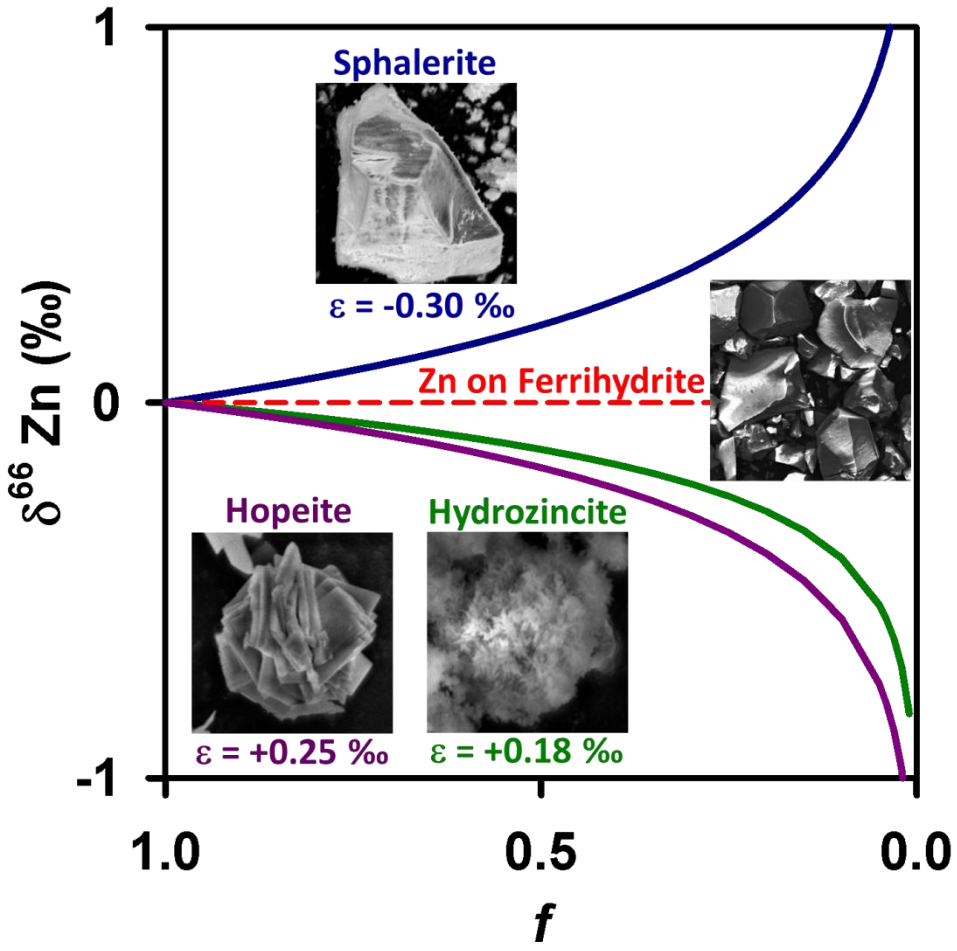

519

Zinc isotope fractionation as an indicator of geochemical attenuation processes

Harish Veeramani[1†*], Jane Eagling[1], Julia H. Jamieson-Hanes[1], Lingyi Kong[1], Carol J. Ptacek[1] and David W Blowes[1]

[1]Department of Earth and Environmental Sciences
University of Waterloo
200 University Avenue West
Waterloo, Ontario
Canada N2L 3G1
*harish.veeramani@uwaterloo.ca

†Present Address:
School of Engineering
University of Glasgow
Glasgow G12 8QQ
United Kingdom
Phone: +44(0)141-330-1839
Email: harish.veeramani@glasgow.ac.uk

SUPPORTING INFORMATION

1. Iron Oxide Synthesis

A batch of 2-line ferrihydrite was synthesized according to the method described by Antelo and co-workers. [1] Briefly, 40 g of unhydrolyzed crystals of $Fe(NO_3)_3$ were dissolved in 500 mL deionized water that was vigorously stirred during the addition of 350 mL of 1 M KOH (pH 7.5). The resulting precipitate was washed ten times by centrifugation (10000 G for 15 minutes) and lyophilized (Labconco) for 24 hours and stored at -20˚C. Each batch of ferrihydrite was used within a week following preparation to prevent phase transformation to goethite. Samples of ferrihydrite were periodically checked by X-ray diffraction (XRD) to ensure the absence of goethite (Figure S1).

2. Zinc Precipitation Experiments

Zinc sulfide was precipitated in a series of batch experiments involving 8 mM $ZnSO_4$ (523 mg L^{-1}) that was amended with varying concentrations of Na_2S_2. An acidic solution of $ZnSO_4$ (pH c.a. 3) was purged for several hours with ultra-pure argon to exclude atmospheric CO_2. The addition of Na_2S_2 to batches of $ZnSO_4$ was carried out gravimetrically in screw-cap centrifuge tubes. The tubes containing the reaction mixture were allowed to stand for 24 hours inside an anoxic glove-box (Coy Laboratory Products, Grass Lake, MI) with occasional shaking.

The precipitation tests for Zn carbonate hydroxide and Zn phosphate were similar to Zn sulfide in that an acidic and anoxic solution of 8mM $ZnCl_2$ was amended with varying concentrations of $NaHCO_3$ and Na_3PO_4, respectively in a series of batch experiments. Although spontaneous Zn precipitation was observed under all test conditions, the centrifuge tubes containing Zn sulfide, Zn carbonate, and Zn phosphate were allowed to remain in the anoxic glove-box for 24 hours prior to centrifugation and filtration. The tubes were centrifuged at 6000 XG for 20 minutes and filtered using 0.2 μm PES filters. The pH of the supernatant was measured and a subset of the filtrate was tested for alkalinity. The remaining filtrate was acidified for bulk aqueous chemistry and isotope analysis. Total alkalinity was

measured using a HACH digital titrator (Model 16900) and titrated with 0.16 N H_2SO_4 to an endpoint of pH 4.5 using bromocresol green-methyl red as a pH indicator.

3. Solid Phase Characterization

3.1 SEM

The morphologies of the Zn precipitates were observed using a Zeiss Ultra scanning electron microscope (SEM) at the Waterloo Advanced Technology Laboratory (WATLab). The Zn precipitates were freeze-dried and the dry powder was loaded onto SEM sample stubs. A layer of carbon tape was applied to the sample stubs before loading the samples. The images were acquired at a working distance of 10 millimeters using an in-lens detector. Selected samples were sputter-coated briefly with Au to minimize sample charging during image acquisition.

3.2 X-ray diffraction (XRD)

The structure of the solid phase precipitates was confirmed using a Bruker D8 Focus X-Ray Diffractometer (XRD) equipped with a Cu Kα source. Measurements were carried out using a step-time of 1s, step-size of 0.05 ranging from 5 to 90 2-theta. Background subtraction and peak identification were carried out using the Diffrac.Suite EVA software.

3.3 Synchrotron powder diffraction (SRPD)

A sample of ferrihydrite was ground in a clean mortar and pestle and loaded into polyimide capillary tubes (Cole-Parmer: 95820-06). The ends of the tube were sealed using glue (Loctite 454) and the samples were analyzed at beamline 08B1-1 (CMCF-BM) at the Canadian Light Source. Diffraction data was collected from 5 to 40 2θ using a wavelength (λ) of 0.688 Å. The data was processed using the GSAS-II Crystallography data analysis software. [2]

4. MC-ICP-MS analysis

Samples were combined with a double-spike solution of known isotopic composition (Isoflex, San Francisco, USA, 67Zn:70Zn = 0.43:0.57, spike:sample ratio of 0.37) and converted to an HCl matrix via evaporation. Spike-sample mixtures were loaded onto columns containing 1.6 mL of AG-MP-1M anion-exchange resin (100–200 mesh; Bio-Rad, USA). Unwanted matrix elements were eluted with progressively decreasing concentrations of HCl; Zn was eluted in 0.5 M HCl during the final step of the purification scheme. The eluted Zn fraction was evaporated and re-dissolved in 5 M HNO_3 twice to ensure complete removal of chlorine ions and converted back to a HNO_3 matrix via evaporation. Each sample was purified in duplicate and the duplicates were analyzed during three analytical events; the final value for each sample was calculated as the average of six replicate measurements. High-precision Zn isotope measurements were performed using a multi-collector inductively-coupled plasma mass spectrometer (MC-ICP-MS; Thermo Scientific Neptune).

Results

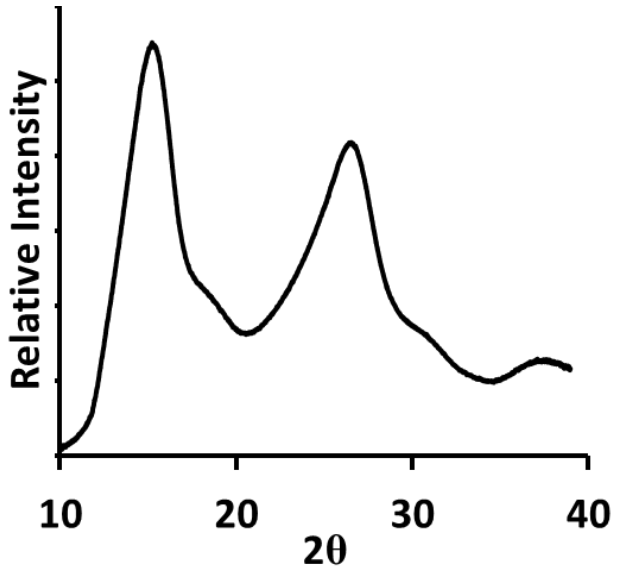

Figure S1: Synchrotron powder diffraction of synthetic ferrihydrite. The diffractogram shows two broad reflections at $2\theta = 15.23$ and 26.55 corresponding to interplanar distances (d-spacing) of d = 2.58 and 1.49 Å respectively. The diffraction pattern is similar to that reported by Carta and coworkers for synthetic 2-line ferrihydrite nanoparticles[3].

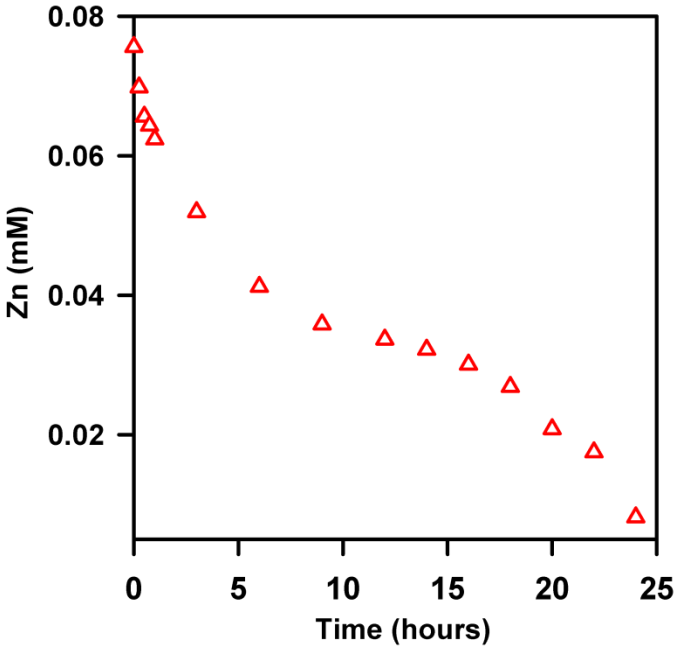

Figure S2: Time-dependent adsorption of Zn on ferrihydrite. The concentration of ferrihydrite was 2.0 grams/L and the pH of the suspension was maintained at 7.2.

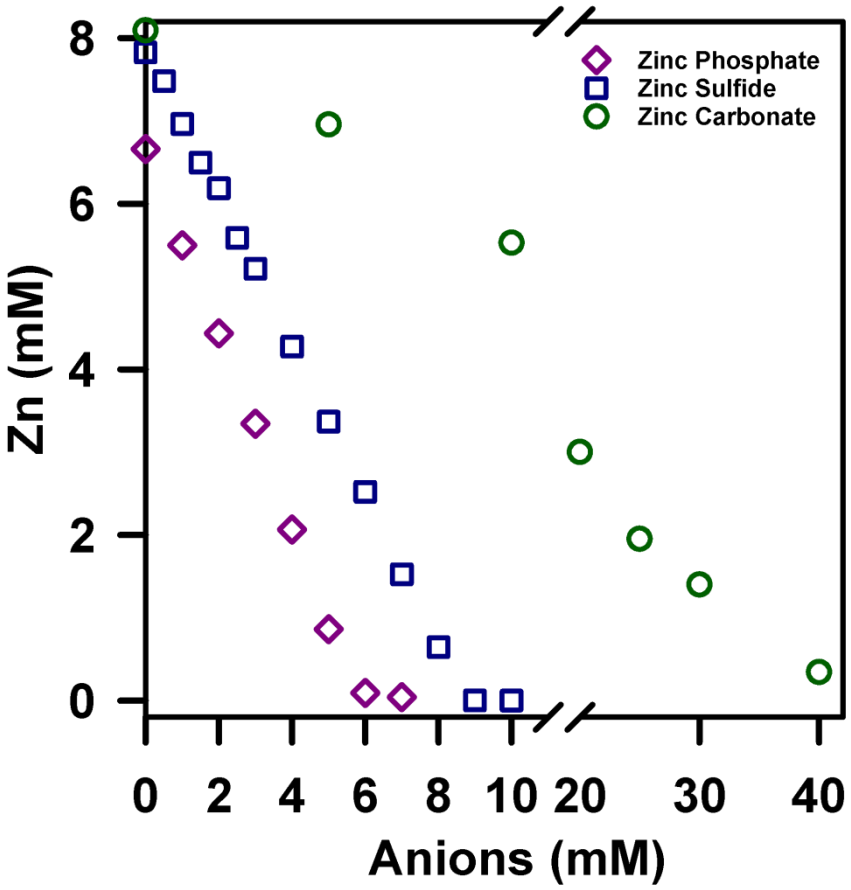

Figure S3: Zinc removal from solution due to precipitation with sulfide(□), carbonate (○) and phosphate (◇).

A

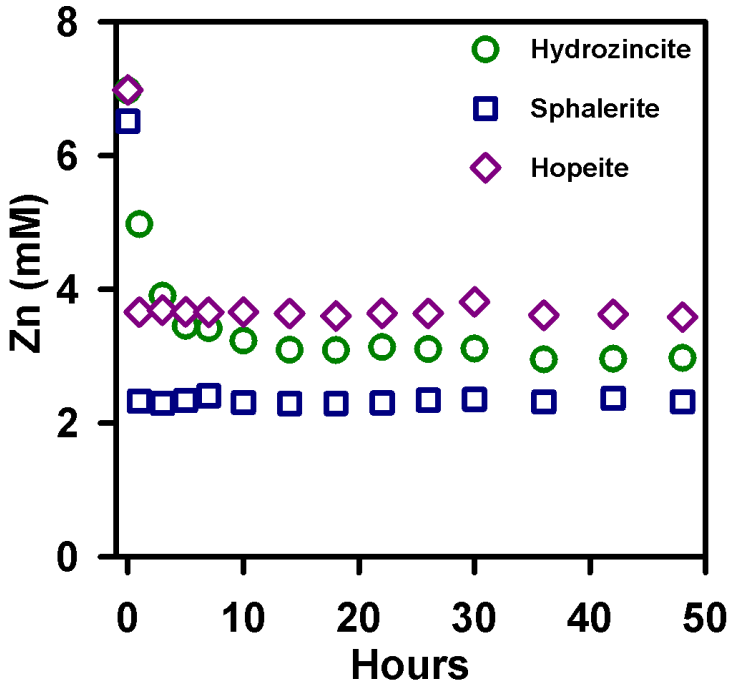

B

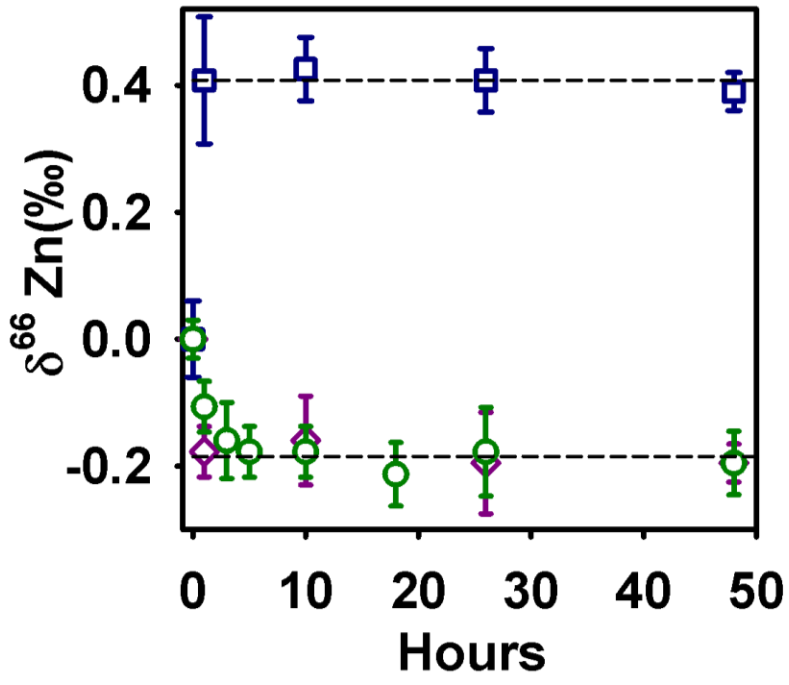

Figure S4: A) Time-dependent precipitation of sphalerite, hopeite and hydrozincite using fixed counter-anion concentration. B) Isotope analysis of selected samples showing isotope equilibrium. Zinc isotope equilibrium was reached immediately during the formation of Sphalerite and Hopeite. In case of hydrozincite, isotope equilibrium was reached within 6 hours.

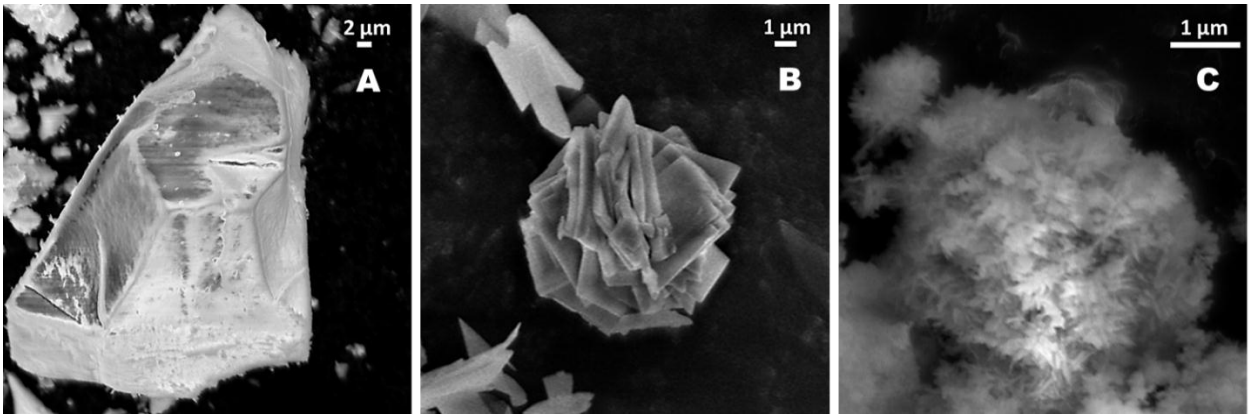

Figure S5: Scanning electron microscopy images of the Zn precipitates; (A) Zn sulfide as sphalerite (B) Zn phosphate as hopeite and (C) Zn hydroxycarbonate as hydrozincite.

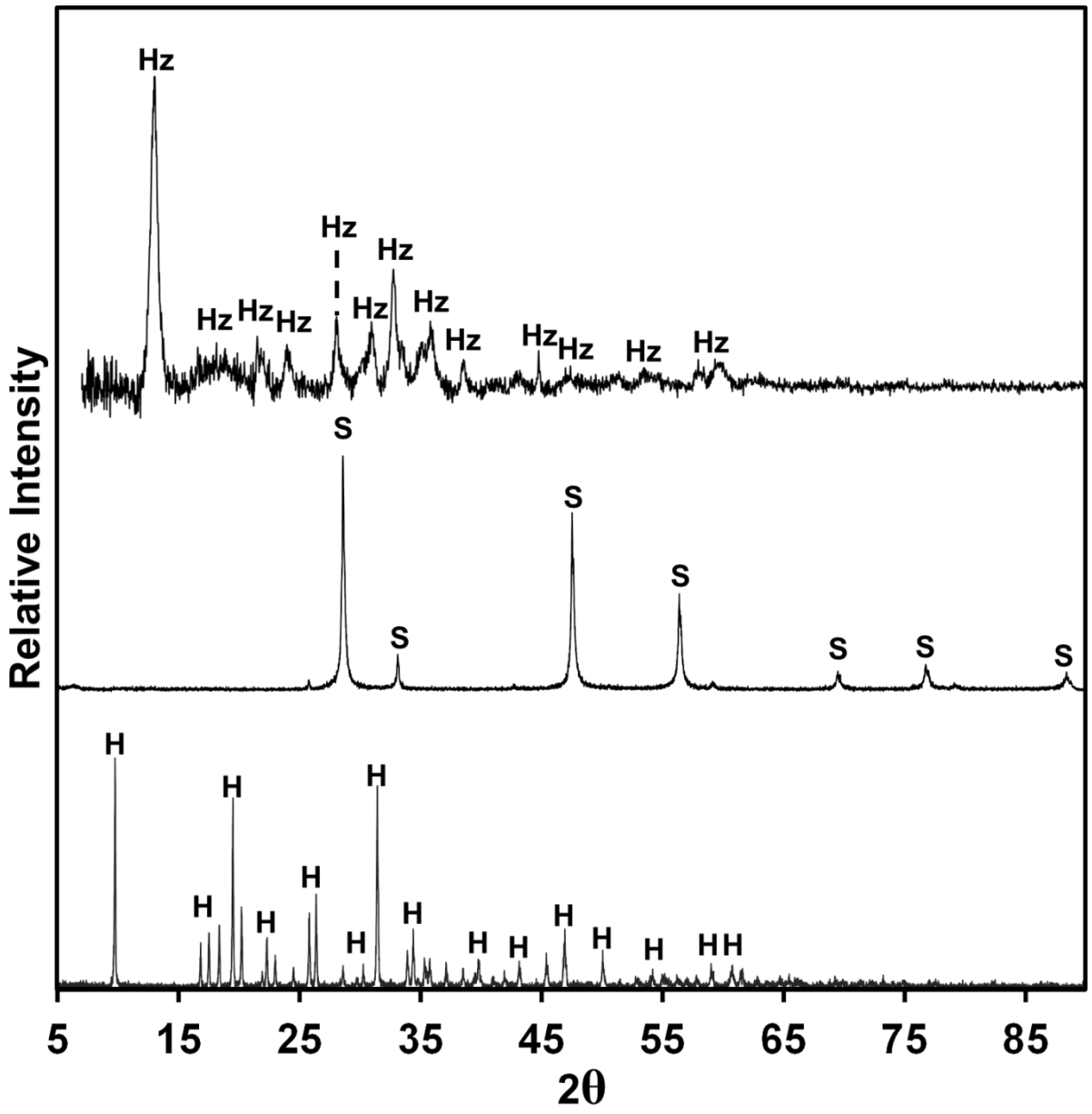

Figure S6: X-ray diffraction confirming the identity of zinc precipitates. The major peaks for each phase is highlighted; hopeite (H), sphalerite (S) and hydrozincite (Hz).

Table S1: Compilation of pH, alkalinity, counter-anion concentration, concentration of Zn and δ^{66}Zn in the reacted solution following zinc precipitation and zinc sorption experiments. (ND = Not Determined)

Phosphate mM	Final pH	Alkalinity as $CaCO_3$ (mg L^{-1})	Zn (mM) Unreacted Solution	δ^{66}Zn Unreacted Solution	2σ (‰)	Carbonate mM	Final pH	Alkalinity as $CaCO_3$ (mg L^{-1})	Zn (mM) Unreacted Solution	δ^{66}Zn Unreacted Solution	2σ (‰)
1	5.71	25	5.5	-0.09	0.07	5	6.63	110	7	-0.05	0.03
2	5.68	44	4.4	-0.2	0.04	10	6.46	195	5.5	-0.09	0.03
3	5.7	50	3.3	-0.25	0.04	15	6.5	280	4.2	-0.16	0.05
4	5.78	59	2.1	-0.34	0.04	20	6.61	417	3	-0.28	0.08
5	6.01	65	0.9	-0.44	0.03	25	6.68	565	2	-0.32	0.09
						30	6.82	825	1.4	-0.37	0.06
						40	6.92	1195	0.3	-0.46	0.1

Sulfide mM	Final pH	Alkalinity as $CaCO_3$ (mg L^{-1})	Zn (mM) Unreacted Solution	δ^{66}Zn Unreacted Solution	2σ (‰)	Ferrihydrite grams L^{-1}	Sampling (Hours)	Zn (mM) Unreacted Solution	Final pH	δ^{66}Zn Unreacted Solution	2σ (‰)
0.5	3.87	ND	7.5	0.07	0.04	2	0	75.6	7.2	-0.14	0.04
1	3.84	ND	7	0.07	0.01	2	0.25	69.8	7.2		
1.5	3.8	ND	6.5	0.09	0.06	2	0.5	65.6	7.2		
2	3.75	ND	6.2	0.14	0.01	2	0.75	64.3	7.2	-0.16	0.04
2.5	3.72	3	5.6	0.12	0.02	2	1	62.4	7.2		
3	3.69	6	5.2	0.14	0.03	2	3	51.9	7.2	-0.2	0.06
4	3.72	10	4.3	0.2	0.03	2	6	41.2	7.2	-0.2	0.04
5	3.83	13	3.4	0.27	0.03	2	9	35.8	7.2		
6	3.96	16	2.5	0.34	0.06	2	12	33.7	7.2	-0.2	0.09
7	7.15	33	1.5	0.41	0.06	2	14	32.2	7.2		
8	10.79	120	0.6	0.5	0	2	16	30.1	7.2	-0.14	0.08
9	11.23	197	0	0.55	0.05	2	18	26.9	7.2		
10	11.45	296	0	0.76	0.05	2	20	20.8	7.2	-0.19	0.01
						2	22	17.5	7.2		
						2	24	8.2	7.2	-0.21	0.05

References

(1) Antelo, J.; Arce, F.; Fiol, S. Arsenate and phosphate adsorption on ferrihydrite nanoparticles. Synergetic interaction with calcium ions. *Chem. Geol.* **2015**, *410*, 53–62.

(2) Toby, B. H.; Von Dreele, R. B. GSAS-II: The genesis of a modern open-source all purpose crystallography software package. *J. Appl. Crystallogr.* **2013**, *46*, 544–549.

(3) Carta, D.; Casula, M. F.; Corrias, A.; Falqui, A.; Navarra, G.; Pinna, G. Structural and magnetic characterization of synthetic ferrihydrite nanoparticles. *Mater. Chem. Phys.* **2009**, *113*, 349–355.

Acknowledgements

The ferrihydrite sample for SRPD was analyzed at the Canadian Light Source during the NSERC TERRE-CREATE training program. The Canadian Light Source is supported by the Natural Sciences and Engineering Research Council of Canada, the National Research Council Canada, the Canadian Institutes of Health Research, the Province of Saskatchewan, Western Economic Diversification Canada, and the University of Saskatchewan.